Radar based horizontal wind profile retrieval techniques: DFT applied to scanning Doppler radar measurements.

N. K. S. Ishwardat



Challenge the future

Radar based horizontal wind profile retrieval techniques: DFT applied to scanning Doppler radar measurements.

by

N. K. S. Ishwardat

to obtain the degree of Master of Science at the Delft University of Technology, to be defended publicly on Wednesday March 8, 2017 at 11:00 AM.

Student number:

4042050 Thesis committee: Prof. DSc. A. Yarovoy Dr. O. A. Krasnov Ir. C. M. H. Unal

TU Delft EEMCS, MS3 chairman TU Delft EEMCS, daily supervisor TU Delft CiTG, researcher A. C. P. Oude Nijhuis MSc. TU Delft EEMCS, PhD candidate

An electronic version of this thesis is available at http://repository.tudelft.nl/.

The cover image is created from a photo made by Micheal Gaida. It can be found on: https://pixabay.com/en/air-bag-wind-sock-weather-sky-1696481/.



Abstract

During this thesis research an attempt is made to introduce a computational lightweight horizontal wind retrieval method applied on scanning Doppler radar velocity data. Horizontal wind parameters are the wind speed and wind direction. If know they are known in a vertical extend, they form a wind profile. In a typical approach, horizontal wind parameters can be obtained through a least squares fit of the measured Doppler radar velocity data. As the least squares fit can be computational costly the discrete Fourier transformation (DFT) is tested in this study. A new method called the Fast Fourier Wind Vector Algorithm or FFWVA is proposed for horizontal wind field determination.

The proposed FFWVA method is based on the Velocity Azimuth Display or VAD. The VAD is a frequency based analysis method mentioned by Doviak and Zrnic. Tests are performed with wind field simulations that have multiple wind layers. These multiple wind layers are common in local weather hazards like vertical wind shears, microbursts and whirlwinds. The tests include validation with wind fields as described in the Doppler velocity interpretation guide of Brown and Wood. Apart from ideal simulations other cases with noise and gaps in the azimuthal scanned velocity data are tested.

The results of an ideal simulation show that the horizontal wind field parameters are determined with negligible error. However, in cases with random gaps in the data or with less than 50% data the FFWVA shows significant errors. The FFWVA wind determination works when the data input is done following a specified manner: either with an even spread of gaps or with exact 50% data available.

Acknowledgment

Today, I am happy to present my thesis as final work for my masters at the Technical University of Delft. Feeling humble performing this research and I would like to express my gratitude to all committee members reading my thesis. With special thanks to Dr. Oleg Krasnov and Prof. Alexander Yarovoy for the opportunity and the time they gave me to finish this research. I would also like to thank Msc. Albert Oude Nijhuis for his help, efforts and always helpful criticism on my work.

In general, I am blessed with the love I receive everyday from my family and friends. This with a special remark to my wife for her patience, understanding and thoughts on my work.

I am forever grateful for the unconditional love, support and encouragement from my mother who has made it possible for me to study for my masters.

Kavish Ishwardat Delft, February 2017

Table of Contents

Ak	Abstract									
Ac	Acknowledgment									
Table of Contents										
1	Introduction 1.1 Motivation									
2	Background 2.1 Wind Hazards and Hazard Underestimation 2.2 Doppler Radar for Weather Measurements 2.3 Linear Wind Model 2.4 Velocity Azimuth Display	7 10								
3	Methods 3.1 Environment Set Up	13 14								
4	Results 4.1 Simulations	30 33 35								
5	Conclusion & Recommendations 5.1 Summery of Results 5.2 Conclusion 5.3 Recommendations sopendices	39								
-	Criteria for KNMI weather warning codes	43								
	Bibliography 4									

Introduction

The first official weather institutes for weather forecasting and the prediction of weather hazards date from the nineteenth century. During that time the United States had established their department for meteorology and weather forecasting. Their main goal was to predict weather storms and the prevention of (economic) losses caused by such storms [1]. Other than such institutes it is know that the Greeks studied the weather in years BC. Therefore it is likely to assume that the interest in weather observation is as old as mankind.

In our current society weather predictions are an essential part of daily life considering that these predictions are done in a more pre-emptive way. Weather predictions are of value for most outdoor activities and essential for industrial sectors such as: aviation, maritime, construction, farming and outdoor festivities. A more personal need for weather predictions can be found in planning a vacation, daily commute or other outdoor activities. Weather predictions are of high value if they contain information on potentially dangerous weather [1, 2, 3].

Dangerous weather conditions have a potential risk to cause economic losses and even loss of human life. Weather predictions can help to minimize this risk by warning pre-emptively. The conditions of dangerous weather and weather hazards can vary in type and intensity. Examples of various weather hazards are rainstorms, cloudbursts, hail, snowstorms, thunderstorms, cyclones, tornadoes. Most of these hazards occur in combination with precipitation and are dangerous at high levels of intensity. The precipitation in these hazards can be measured and detected with the help of radar (radio detection and ranging). Weather radars measure with high spatial and temporal accuracy and can be used for weather forecasts and for weather hazard detection.

In the next section the need for fast processing weather algorithms will be discussed with help of a weather warning systems explanation. After that the state-of-the-art will be covered and in the last section the research goals for this thesis will be explained.

1.1. Motivation

With a trade-off for accuracy, the current technologies allow for measurements in most weather scales that are indicated in Table 1.1. For example in the American WSR-88D radar network, known as NEXRAD, the individual radar sites can measure reflectivity up to a range of 460 km and measure velocities up to 230 km [4, 5]. These measurement ranges will vary upon the chosen radar specifications. Larger areas can be covered by synthetic measurements of multiple radars sites in such radar networks. In a normal straight forward case, equipment set up for microscale will measure with short temporal update intervals and with high spatial resolution. The combination of these short update intervals and a high resolution system is complex. This combination requires an increased amount of data storage and data processing at the individual radar sites. The complexity that is paired with the high computational demands could be a reason for the lack of microscale warning systems [6].

To further elaborate on the complexity of forecasting in microscale, the effects of the resolution of a measurement and/or prediction should be known. During the analysis of (severe) weather a low resolution measurement or prediction can cause for hazards to be underestimated or missed. The reason for this underestimation is that the measurements are an average of the measured area where

Classification	۱	Location scale	Duration scale
Macroscale	α β	> 10.000 km 2.000 - 10.000 km	days to months
Mesoscale	α β γ	200 - 2.000 km 20 - 200 km 2 - 20 km	hours to days
Microscale	α β γ	200 m - 2 km 20 - 200 m < 20 m	minutes to hours

Table 1.1: The classification of macro-, meso- and microscale according to Orlanski [7]. With α , β , γ sub-classification.

high intensity levels could be filtered out. Both direct measurements and simulations with forecast models (predictions) can suffer from this underestimation problem depending on the resolution.

An approach for a microscale warning system would be to set up a radar sensor network with multiple independent measurement sites (nodes). Each node should perform high resolution measurements for a small portion of the entire measurement area altogether improving the resolution problem. The information from the independent nodes can be gathered to create an overview of the entire area. Also setting up multiple smaller measurement sites (nodes) tend to be more cost effective compared to a single 'high-end' site. However this approach with high resolution measurements for each node will require simplified data processing algorithms as timely updates are required.

1.2. State-of-the-Art

As motivated in the previous section a microscale weather warning system would need lightweight detection algorithms. During this thesis the choice is made to focus on wind hazard detection through wind profiling. For wind estimations in a non-linear and dynamic wind simulation near objects, computational fluid dynamics (CFD) is often applied. CFD is based on numerical analysis techniques which calculates the state of an entire simulation environment in smaller pieces. For example weather forecasting models, often referred to as numerical weather prediction (NWP), also use numerical analysis techniques but are applied on a larger scale. Numerical analysis techniques can be very detailed upon the chosen simulation setting but are complex, time-consuming and computationally costly. This makes a numerical analysis method impractical for a weather warning system as timely updates are required.

Another approach for the determination of wind profiles and their wind velocity vectors is commonly done with a linear approach. For measurements with a single Doppler radar a linear approach is described by Doviak and Zrnic [4]. As the name implies this method is valid for wind fields that are assumed to behave linearly. This method for wind vector determination will be further referred to as the linear wind model (LWM). The LWM can be used to determine needed wind velocity vectors at unknown spatial points in a volume and will be explained in section 2.3. This approach needs a least squares fit which can also be computationally costly.

A different approach is to determine the wind profiles and their wind vectors through the Velocity Azimuth Display (VAD) method. When plotting the radial velocities to the azimuth a characteristic sinusoidal shape is visible. This sinusoidal shape is exploited and processed as a harmonic with a Fourier Series. The VAD method is valid for linear wind fields as explained by Doviak and Zrnic [4] and can determine the horizontal wind direction and speed. The linear wind assumption can account for most observed wind varieties and the linear assumption is also needed for interpreting data from a single Doppler site [4]. The VAD method is less advanced than a numerical analysis method or the LWM as it only determines the horizontal wind parameters.

1.3. Problem Definition

With the idea of a microscale weather warning system a fast updating (lightweight) horizontal wind determination algorithm is required. The approach for such a system has been explained in section

1.1. With the choice for wind anomaly research, existing methods for horizontal wind determination were explained in section 1.2.

This thesis research proposes a frequency based analysis method that determines horizontal wind parameters through the discrete Fourier transform (DFT). The explained VAD method is the foundation of this proposed method as it also is such a frequency based analysis method. Both exploit the sinusoidal characteristic of azimuthal Doppler radar round scans. The difference is that the VAD method only calculates the needed Fourier coefficients of interest through a Fourier series. This in opposite to the proposed method that calculates the complete frequency spectrum through the DFT.

The DFT has various efficient algorithms referred to as the fast Fourier transform (FFT) which makes this an interesting approach. The DFT will be covered in subsection 3.4.2.

The hypothesis is that the DFT could have a positive effect on data processing because of the usage of current FFT algorithms. The proposed method could also lead to new insights in multi-layered wind field determinations because of the available (complete) frequency spectrum. The thesis statement is formulated as follows.

An on a discrete Fourier transform based VAD approach can be used to perform wind field measurements and retrieve the horizontal wind speed and direction from an azimuthal Doppler radar scan.

The research questions used to determine this are:

- What is the performance of horizontal wind determination when the Fourier series is replaced with a DFT, based on the VAD method?
- Can such a frequency based processing method measure and detect multi-layered wind fields?

The thesis outline is as follows: In chapter 2 basic theory and explanations of these theories are given. Afterwards in chapter 3 the proposed method and simulation setup are discussed. In chapter (4) the proposed method is tested and compared to the LWM with gaps and noise in the simulation data.

 \sum

Background

This chapter will cover the basic theory and formula's used to give a better understanding of the thesis research. In the first section weather hazards and their scales are covered to explain the underestimation problem in more detail.

Then a basic explanation of radar operation and its retrieval formula's will be discussed. This will help to understand the used simulation parameters and noise simulation. The determination of the radar Doppler velocity is of high interest as it is the input for the proposed analysis method. The input Doppler velocity data is retrieved from either simulation or from a post processed data set of real radar measurements. However the simulation set up is covered as a separate section in the next chapter (3.2).

This chapter will also cover two horizontal wind determination models: the velocity azimuth display (VAD) and linear wind model (LWM). The horizontal wind is commonly known as 'the wind' and both determination models will be explained in more detail. The VAD is used as foundation for the proposed frequency based analysis method. The LWM is used to create and simulate complete wind fields and can also be used as a horizontal wind determination method. The horizontal wind determination of the LWM is performed with the least squares method and is also explained. The LWM is used in the results chapter (4) as a comparison to the proposed method.

2.1. Wind Hazards and Hazard Underestimation

Wind is one of the weather hazards that can have a tremendous impact in areas with a high-density population or crowd like metropolises and large festivals. An overview of other weather hazards with their scale classification is available in Table 2.1. A wind shear is one of the dangerous winds and is described as a sudden change of wind speed and/or direction in for example microbursts or whirlwinds. A schematic of a microburst is shown in Figure 2.1. Visible is a microburst causing a vertical wind shear near the ground. In the table wind shears are indicated under microbursts and classified in the lower mesoscale γ . However wind shears also exist in the more difficult to forecast microscale and for this reason are of high interest. As explained the microscale hazards, like these wind shears with multiple wind layers, are difficult to measure and predict. The existence of multiple wind layers with different speeds and/or directions will be referred to as a multi-layered wind field.

The resolution problem explained earlier exists if low resolution measurements cause for (hazard) underestimation. An example of such an underestimation is shown in Figure 2.2. Visible is that the high intensity area is wider than the low resolution measurement indicates. Another example is the criteria table of the Dutch national weather alarm, available in Dutch as Appendix A. The criteria table indicates that warning code orange will be given for hazard forecasts in areas larger than 50 km x 50 km that happen within 12, 24 or 48 hours. If the area criterion is not met for the forecast the warning will be a lower code yellow, and thus with a higher risk of hazard underestimation. These examples show that the source of the hazard information makes no difference in the essence of this underestimation problem.

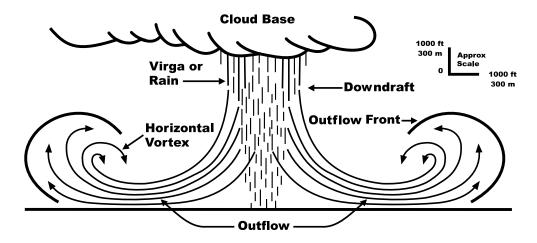


Figure 2.1: Cross section of a microburst. Visible are a downdraft, front gust (left) and back gust (right). [8].

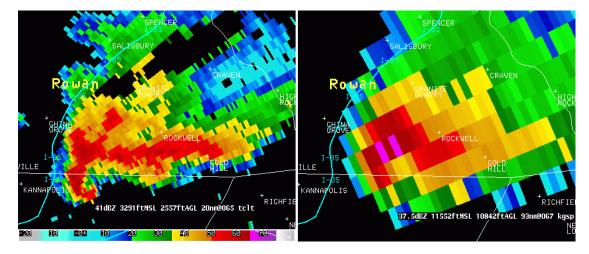


Figure 2.2: Comparison of two different Doppler radars systems: TDWR and NEXRAD. "Located in near identical locations, a TDWR return (left) and NEXRAD return (right) showing the improved resolution in reflectivity, also showing the attenuation in the TDWR due to absorption from heavy precipitation as a black gap." Quote from Wikipedia and images from weather.org [9, 10].

Disturbance	Scale	Duration	Maximum wind	Classification
Extratropical cyclone	500 - 2000 km	3 - 15 days	55 m s ^{-1}	Macroscale
Cold front	500 - 2000 km	3 - 7 days	25 m s ^{-1}	Macroscale
Anticyclone	500 - 2000 km	3 - 15 days	10 m s ^{-1}	Macroscale
Warm front	300 - 1000 km	1 - 3 days	15 m s ⁻¹	Mesoscale α
Hurricane	300 - 2000 km	1 - 7 days	90 m s ⁻¹	Mesoscale α
Tropical cyclone	300 - 1500 km	3 - 15 days	33 m s ⁻¹	Mesoscale α
Tropical depression	300 - 1000 km	5 - 10 days	17 m s ⁻¹	Mesoscale α
Dry front	200 - 1000 km	1 - 3 days	20 m s ⁻¹	Mesoscale α
Midget typhoon	50 - 300 km	2 - 5 days	50 m s^{-1} 25 m s^{-1} 35 m s^{-1} 60 m s^{-1} 55 m s^{-1} $-$	Mesoscale β
Mesohigh	10 - 500 km	3 - 12 h		Mesoscale β
Gust front	10 - 300 km	0,5 - 6 h		Mesoscale β
Mesocyclone	10 - 100 km	0,5 - 6 h		Mesoscale β
Downslope wind	10 - 100 km	2 - 12 h		Mesoscale β
Supercell storm	20 - 50 km	2 - 6 h		Mesoscale β
Cumulonimbus	10 - 30 km	1 - 3 h		Mesoscale β
Macroburst	4 - 20 km	10 - 60 min	40 m s ⁻¹	Mesoscale γ
Cumulus	2 - 20 km	10 - 100 min	-	Mesoscale γ
Microburst	2 - 20 km	10 - 100 min	70 m s ⁻¹	Mesoscale γ
Tornado	2 - 20 km	10 - 100 min	100 m s ⁻¹	Mesoscale γ
Suction vortex	5 - 50 m	5 - 60 min	140 m s ⁻¹	Microscale
Dust devil	1 - 100 m	0,2 - 15 min	40 m s ⁻¹	Microscale

Table 2.1: Weather hazards in the lower atmosphere with scale classification [11]. The lower atmosphere or troposphere is where most weather phenomena occur. The troposphere it is the lower 10 to 20 km of the atmosphere.

2.2. Doppler Radar for Weather Measurements

Radar technology is very broad applied with numerous applications in aviation, automotive, maritime, military and meteorology. Typical radar applications are car speed measurements, air traffic surveillance with collision avoidance and distance measurement systems in maritime and automotive. Techniques like sonar, lidar and medical ultrasounds are fundamentally similar techniques as radar, but with the key difference that they operate in different frequency bands. Doppler radar can be implemented as a weather radar and measure wind velocities from different directions. The results of these wind measures are called wind profiles and can be used as input for weather forecasting.

2.2.1. How Doppler Radar Works

A basic explanation of radar is the detection of an object by transmission of an electromagnetic wave and measuring the echoes of the reflecting waves. A still general but more comprehensive explanation in the case of a weather radar is as follows:

- An antenna system sends out electromagnetic signals.
- The radar measures echoes of the reflected signal. These reflections are caused by objects referred to as scatterers or hydrometeors.
- The travel time of the echoes received back at the radar site corresponds with the distance between the radar and the hydrometeors.
- The sent signals can be varied in length, rate and/or frequency in order to differentiate the sent signals. These techniques help to prevent range and velocity ambiguity.
- Polarization information describes the electromagnetic plane components of sent and received signal and can help to differentiate the hydrometeors.

 In the case of a Doppler radar, the frequency change between the sent and received signal is measured and corresponds with the radial velocity of the hydrometeors.

Reflecting hydrometeors are under the influence by the surrounding wind field, and the measured velocities correspond with the surrounding wind speed. The measured velocities can be plotted at their measured distances to describe the wind flow at various heights or ranges, a wind profile. Another way to display the measured Doppler velocity data is to plot it to the horizontal measurement angle (looking direction) called the azimuth. An example of such a plot is shown in Figure 2.3 with a Westerly wind blowing from West to East. The data visible in this figure is the Doppler velocity data of a radar round scan that be analyzed as a harmonic as proposed by Browning and Wexler [12]. Now that basic radar operation is explained the next section will cover the theory in more detail and in relation to the performed simulations.

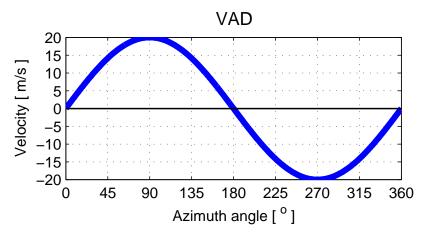


Figure 2.3: Velocity data plotted to the azimuth with an example of a simulated radial wind speed of 20 m/s from the West to the East.

2.2.2. Doppler Radar equations

The mean Doppler velocity v_d is the output parameter of interest during this research and is also referred to as the radial velocity v_r . In order to process and simulate radar data sets the range, resolution and beam width of the radar should be understood as the weather radar measures echoes of a volume. As mentioned in the previous section the range can be determined through the round-trip time of an echo. The measured round-trip time τ_{rtt} of an echo is described as,

$$\tau_{rtt} = \frac{2r}{c} = \frac{r_{rt}}{c}.$$
(2.1)

Where:

τ_{rtt}	=	Round-Trip Time	[s] ,
r	=	Range	[m],
r _{rt}	=	Range (round-trip)	[m].

In free space the described travel speed *c* of the pulse is equal to the speed of light $(3 \cdot 10^8 \text{ m s}^{-1})$. In the case of a pulsed radar its defined with a Pulse Repetition Frequency (PRF) that describes the time between the sent measurement pulses (i.e. sample time). The chosen PRF is of interest as it determines the maximum detection range r_{max} or maximum ambiguous range of the pulsed radar. The PRF is described by Doviak and Zrnic [4] as,

$$r_{max} = \frac{c}{2PRF}.$$
(2.2)

Where:

r _{max}	=	Maximum detection range of radar	[m] ,
С	=	Travelling speeds of the pulse	[m/s] ,
PRF	=	Pulse Repetition Frequency	[Hz].

A constant PRF value will cause ambiguity between echoes inside the r_{max} range and echoes that are outside the r_{max} range [4]. This ambiguity can be challenged by active variation of the PRF but will not be used during this research, see Brown and Wood [13] for more details. The pulse width τ directly relates to the range resolution ΔR . Scatterers that are spaced at a distance smaller than the range resolution are detected as a single subject by the radar. The range resolution can be improved with pulse compression [4]. For applications that suffer from this range resolution problem of a pulsed radar the Frequency Modulated Continues Wave (FMCW) radar is an alternative option. The beam width is a radar antenna specification and is also referred to as the full width at half maximum (FWHM) and can vary for the azimuth and elevation direction.

The intensity of the received volumetric echo can be described with the radar reflectivity factor *Z* which is of high interest for weather radars also. The reflectivity factor *Z* is determined through the received signal power P_r measured by the radar. The reflectivity factor *Z* is influenced by various parameters like for example the rainfall rate and the particle size distribution. Although the reflectivity factor itself is not of direct interest for this research the formula used to determine it is: the 'radar equation'. A basic radar equation is shown as equation 2.3 but the radar equation can be written in many forms. Another radar equation is for example the weather radar equation shown in equation 2.4 [4]. Note the difference between these radar equations with reflectivity *Z* instead of a Radar Cross Section (RCS) σ . As the reflectivity is a volume based metric it reduces the range dependence from r^{-4} to r^{-2} . The received signal P_r is needed for the Doppler velocity determination and is under influence of the reflectivity factor and various radar parameters:

$$P_{\rm r} = \frac{P_{\rm t}G_{\rm t}G_{\rm r}\sigma\lambda^2 L_{\rm s}}{(4\pi)^3 r^4}.$$
(2.3)

Where:

Whoro.

$P_{\rm r}$	=	Received power	[W] ,
$P_{\rm t}$	=	Transmit power	[W] ,
$P_{\rm t}$	=	Received power	[W] ,
$G_{\rm t}$	=	Gain transmit antenna	[-] ,
$G_{\rm r}$	=	Gain receive antenna	[-] ,
σ	=	Radar cross section	[<i>m</i> ²],
L_{s}	=	System losses	[-].

$$P_r = \frac{\pi^3 P_t G^2 \Theta^2 c\tau |K|^2 Z}{2^{10} \ln(2) \lambda^2 r^2 L_{atm}^2 L_{MF}}.$$
(2.4)

whiche.			
G	=	Gain (receive = transmit) antenna	[-] ,
Θ	=	Antenna beam width	[rad] ,
Κ	=	Precipitation factor	[-] ,
Ζ	=	Reflectivity	[rad] ,
Κ	=	Precipitation factor	[-] ,
λ	=	Wavelength of signal	[m] ,
L_{atm}	=	Atmospheric attenuation from radar site to-	[-] ,
		wards the echo	
L_{MF}	=	Matched filter loss	[-].

The velocity of a scatterer can be measured through the Doppler frequency which in case of radar is the frequency change between the sent signal and the measured echo. This measurement is possible with a coherent set up that has the phase of the sent signal synchronized at the receiver stage. A synchronous detector enables sampling an echo at two instances: with an 'in-phase' and a 'quadrature' component preserving phase information. The Doppler frequency f_d can be expressed in terms of the radar wavelength λ and the radial velocity v_r (Doppler velocity) of the scatterer as,

$$f_d = 2v_r / \lambda. \tag{2.5}$$

For weather radars this radial velocity is the mean velocity of the sampled volume moving in direction of the radar. Just as the determination of the maximum range a maximum velocity can be defined for

the Doppler measurement. The maximum velocity that can determined unambiguously is described as,

$$v_{\max} = \pm \frac{\lambda}{4T_s} = \pm \frac{\lambda \text{PRF}}{4}.$$
(2.6)

where:

$v_{\rm max}$	=	Unambiguous velocity	[m/s] ,
T_s	=	Pulse repetition time (PRT)	[s].

Velocities that are outside the unambiguous velocity range of $\pm v_{max}$ are folded with multiples of $2v_{max}$. This is also known as velocity aliasing or Doppler folding and an example of this can be found in a report of Brown and Wood [13]. Just as the range ambiguity, velocity ambiguity is also improved with an active variation of the PRF. Doppler velocity ambiguity is undetectable without additional data, but a straight forward method to do so is by referencing data points and preventing discontinuities in spatially spread data points [13].

In pulsed radar systems the sent and received power is typically lower than in a continues wave system. The lower power will lead to a lower detection ratio as the detection threshold is harder to reach and the received signal will have larger variance. Multiple received pulses can be integrated to have a better detection ratio due to a better signal-to-noise ratio (SNR) and lower variance, this technique is known as pulse integration. The total integration time can be explained as the measurement time and in combination with the SNR approximates the root mean square (RMS) error of the Doppler velocity. The RMS error in the Doppler velocity is described by Kingsley and Quegan [14] as,

$$\delta v_r \approx \frac{\lambda}{2t\sqrt{2\mathrm{SNR}}}.$$
 (2.7)

Where:

δv_r	=	Radial velocity error	[m/s] ,
t	=	Integration time	[s].

Here $\lambda/2t$ is the radial velocity resolution Δv_r , and the signal-to-noise ratio is described in the next section (3.3). The ambiguous velocity as shown in Equation 2.6 is based on a maximum phase difference between two measured signals. The noise for that signal can be generated complex with a random phase noise in the domain $< 0, \pi >$. The amplitude of this complex value determines the noise power and is expected to have a Gaussian distribution. The noise for this signal and the approach to model this will be explained in a separate section in the methodology chapter (3.3). These formula's are basic radar operation needed for the simulations of radar retrievals, the implementation of these retrievals is explained in chapter 3.1.

2.3. Linear Wind Model

The linear wind model enables measurement of the horizontal wind and also of wind vectors at unknown spatial points. With this model the assumption is that the wind speed varies linearly in all directions: on both the vertical altitude plane *z* as on the horizontal distance plane *x* and *y*. First the general model that can be used for the estimation of wind vectors at unknown spatial points is explained. In contrast with the horizontal wind estimation (2D) this general model is in three dimensions (3D). Mentioned by Doviak and Zrnic [4] the wind vector $v(r, \theta_e, \phi)$ is well represented by a first order Taylor series around the centre of the analysis volume (x_0, y_0, z_0) and described as,

$$\mathbf{v}(x,y,z) = \mathbf{v}(x_0,y_0,z_0) + \frac{\partial v}{\partial x}(x-x_0) + \frac{\partial v}{\partial y}(y-y_0) + \frac{\partial v}{\partial z}(z-z_0).$$
(2.8)

Where:

$$\begin{aligned} x &\approx r \cos \theta'_{\rm e} \sin \phi, \\ y &\approx r \cos \theta'_{\rm e} \cos \phi, \\ z &= (a_{\rm e}^2 + r^2 + 2ra_{\rm e} \sin \theta_{\rm e})^{1/2}. \end{aligned} \tag{2.9}$$

A matrix notation can be introduced from the radar to point $(r, \theta_e, \phi) = v_r(r, \theta_e, \phi) = PK$ and is explained by Oude Nijhuis et al. [15] in more detail. It is described as,

$$P = \begin{bmatrix} \cos \theta'_{e} \sin \phi \\ \cos \theta'_{e} \sin \phi (x - x_{0}) \\ \cos \theta'_{e} \sin \phi (z - z_{0}) \\ \cos \theta'_{e} \cos \phi \\ \cos \theta'_{e} \cos \phi \\ \cos \theta'_{e} \cos \phi (y - y_{0}) \\ \cos \theta'_{e} \cos \phi (z - z_{0}) \\ \cos \theta'_{e} \left[r \cos \theta'_{e} \sin \phi \cos \phi - \frac{1}{2} \left(x_{0} \cos \phi + y_{0} \sin \phi \right) \right] \\ \sin \theta'_{e} \\ \sin \theta'_{e} (x - x_{0}) \\ \sin \theta'_{e} (y - y_{0}) \\ \sin \theta'_{e} (z - z_{0}) \end{bmatrix}.$$
(2.10)

And,

$$\mathbf{K}^{\mathrm{T}} = \left(u_{0}^{\prime}, u_{x}, u_{z}, v_{0}^{\prime}, v_{y}, v_{z}, u_{y} + v_{x}, w_{0}, w_{x}, w_{y}, w_{z}\right).$$
(2.11)

Note that if the range r is relatively small compared to earth effective radius a_e it can also be ignored $(r << a_e)$. An example of a manipulation is for horizontal wind field determination, in that case the elements u_z , v_z and w_z are ignored. The remaining subset of vectors is sufficient and the matrix notation helps to manipulate elements of P & K. For such a case where these can be ignored the elements can be set to zero effectively only using the remaining elements of interest.

The manipulation of the linear wind model is covered in order to use it for determination of (horizontal) wind fields. The retrieved model for v_r using the horizontal these wind vectors is described as,

$$v_{\rm r} = v \cdot (\hat{i}\cos\theta_{\rm e}\sin\phi + \hat{j}\cos\theta_{\rm e}\cos\phi + \hat{k}\sin\theta_{\rm e}),$$

= $u\cos\theta_{\rm e}\sin\phi + v\cos\theta_{\rm e}\cos\phi + w\sin\theta_{\rm e}.$ (2.12)

Where:

v	= \	Wind vector of hydrometeor	[m/s] ,
θ_e	= [Elevation angle of radar	[rad] ,
ϕ	= /	Azimuth	[rad] ,
и	= >	x-component of vector $v_{\rm r}$	[m/s] ,
v	= y	y-component of vector $v_{\rm r}$	[m/s] ,
W	= 2	z-component of vector $v_{ m r}$	[m/s].

The equation is a projection of vector v onto r, the vector from the radar to point described with the spherical radar coordinates (r, θ_e, ϕ) . For determination of the horizontal winds (2D) the vectors u, v are sufficient.

With these simplifications the next step is determination of two-dimensional Cartesian velocity vectors u, v in a reversed manner. This can be done by linearly solving with at least two locations of v_r with their know locations. Two data points are sufficient when assuming a homogeneous vertical wind distribution and thus neglecting the vertical w component. When the vertical wind vector w is not accounted for the radial velocity equation 2.12 reduces to,

$$v_{\rm r} = u\cos\theta_{\rm e}\sin\phi + v\cos\theta_{\rm e}\cos\phi. \tag{2.13}$$

For determination of u, v from measured data, linear solving will not have a direct solution due to inaccuracies. The first inaccuracy is caused by the overdetermined system of the radar measurement. In order solve u and v an equation with two known points would be enough. However the radar retrieves velocity data from multiple directions creating an system with more then two known data points. A system with more data points than needed to solve it is considered to be an overdetermined system. Overdetermined systems are common to lack a single solution. Other inaccuracies are the error in the reflectivity-weighted radial velocity $\epsilon(\hat{v}_r^h)$ and an error in the terminal fall speeds $\epsilon(\hat{w}_r)$, for more information on these errors see Doviak and Zrnic [4]. An alternative to linear solving is to estimate a solution with the least squares method and is common for overdetermined systems [16].

The linear least squares method minimized the sum of the error in solution. The linear least squares method that can be used for determination of u, v is,

$$Ax = b,$$

$$A^{T}Ax = A^{T}b,$$

$$\hat{x} = (A^{T}A)^{-1}A^{T}b.$$
(2.14)

With,

$$\mathbf{b} = \begin{bmatrix} v_{r_1} \\ v_{r_2} \end{bmatrix}, A = \begin{bmatrix} \cos \theta_{e_1} \sin \phi_1 & \cos \theta_{e_1} \cos \phi_1 \\ \cos \theta_{e_2} \sin \phi_2 & \cos \theta_{e_2} \cos \phi_2 \end{bmatrix}.$$

Here \hat{x} is the least square solution of x containing the estimate of u, v. The horizontal wind speed and direction are described as,

$$v_h = \sqrt{u^2 + v^2},$$
 (2.15)

$$\theta = \frac{3\pi}{2} - \arctan \frac{u}{v}, \quad \text{when } v \text{ is negative,}$$

= $\frac{\pi}{2} - \arctan \frac{u}{v}, \quad \text{when } v \text{ is positive.}$ (2.16)

The arctan in equation 2.16 can be replaced with the atan2 function found in most programming languages, finding the correct quadrant and dealing with divisions by zero. The least square method applied to the linear wind model will be referred to as the LWM method and is the estimation of horizontal wind parameters v_h and θ through u and v.

2.4. Velocity Azimuth Display

The Velocity Azimuth Display (VAD) can be considered as a frequency based analysis method due to the determination of the wind direction and speed through a Fourier series. With the VAD method a radar round scan with Doppler velocities is processed as harmonic data but does not relate to a physical frequency. In addition the assumption is that the vertical wind vector w that represents the fall speed is homogeneous for the entire round scan. The VAD explains that the radial velocity, as earlier described in equation 2.12, can be written as the following Fourier series,

$$v_{\rm r} = \frac{1}{2}a_0 + \sum_{n=1}^{\infty} (a_n \cos(n\beta) + b_n \sin(n\beta)).$$
(2.17)

Where:

$$a_1 = -u \cos \alpha,$$

$$b_1 = -v \cos \alpha.$$

As indicated with a_1, b_1 only the first Fourier coefficients is of interest and not the complete Fourier decomposition. Doviak and Zrnic [4] and Browning and Wexler [12] both describe the VAD method and explain that the 'zeroth' coefficient can be used for horizontal wind divergence determination and the second coefficient for deformation determination. The horizontal wind speed and direction can be determined with the determined u, v, see equations 2.15 and 2.16. Important to understand is that the VAD approach requires round scan velocity data from a constant elevation angle and data points that are symmetrically spaced in the azimuth direction.

3

Methods

This chapter will elaborate on the idea of a frequency based analysis method for wind speed and direction determination in more detail. First a framework is set up for the used environment where the used symbols and their spatial directions will be defined. Then the wind field simulations are explained with their inputs wind profiles and the integration of a radar simulation tool called Zephyros. Zephyros is a versatile Doppler radar simulation tool designed by Albert Oude Nijhuis for 4D-Var research. The tool is still under development and the current version is available online [17]. An overview of the used simulation environment will be explained and cover the interactions between the proposed method in Matlab and Zephyros. The operation of the proposed method is explained with a discrete Fourier transform (DFT) calculation example.

3.1. Environment Set Up

In order to keep the data representation consistent the geometry of the (simulation) environment will be defined. A schematic of a scanning (Doppler) radar is shown in Figure 3.1. Visible are the azimuth angle ϕ and elevation angle θ_e . Indicated is that the azimuth angle is measured from the North in a clockwise manner as common in meteorology. Also indicated are the radial velocity v_r and the horizontal wind vector v_h . Positive velocities and wind vectors represent a measured velocity in a radial direction moving away from the radar. Negative velocities represent a measured velocity in a radial direction towards the radar. As explained in the radar section (2.2) the measured velocity will vary based upon the looking position of the radar (the azimuthal angle ϕ). An overview of the measured velocities at their spatial position can be plotted in a 2D radar round scan plot. This type of plot is known as a plan position indicator (PPI). An example PPI is available in the next section (Figure 3.4) where North is at the top axis (positive y) and East at the right axis (positive x). Observe that as azimuth angle $\phi = 0^\circ$ is measured from the North and starts at the positive y axis.

In meteorology wind directions are indicated by the name of the direction it's moving from while vectors are indicated in the direction their moving towards. The wind direction ϕ_{wd} will be defined in the domain $< -180^{\circ}, 180^{\circ} >$. The domain-definition with respect to the meteorological azimuth angle θ is done in Table 3.1. As an example observe that at position $\phi = 270^{\circ}$ a Westerly wind ($\phi_{wd} = -90^{\circ}$ is moving from West to East, and a Doppler radar measuring in that azimuth direction will measure a negative velocity.

3.2. Simulation of Wind Fields

The simulation of wind fields is needed to develop and test the proposed analysis method on known modelled data. In order to simulate wind fields a starting point with reference values is defined as a grid of input wind vectors. These wind vectors indicate the wind direction and speed at known spatial points inside the simulated radar volume. An example of a starting point is shown in Figure 3.2 as input grid. Visible are wind vectors plotted as graph and their numerical values in the table. Similar figures will be used in the results chapter for other simulated wind fields to indicate the wind profile used as input grid.

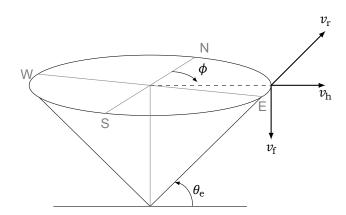


Figure 3.1: Scanning radar overview with meteorological azimuth from the North indicated as ϕ and the elevation angle as θ_e . The radial fall and horizontal velocity vectors indicated as v_r , v_f and v_h respectively.

Wind direction	Azimuth $\angle \phi$		Wind direction $\angle \phi_{wd}$	
	[°]	[rad]	[°]	[rad]
Northerly	0	0	0	0
Easterly	90	$\pi/2$	90	$\pi/2$
Southerly	180	π	± 180	$\pm\pi$
Westerly	270	$3\pi/2$	-90	$-\pi/2$

Table 3.1: Fixed azimuth angle with different wind directions throughout this document.

The calculations for the simulation of the wind fields are performed with Zephyros. Zephyros simulates a needed wind field by calculation of the radars output parameters. The simulated radar output parameters are used as input for the proposed analysis method. For simulations only the volume bins in the measurement area of a radar are of interest. These volume bins are one of the inputs required to simulate with Zephyros as it forms the simulation grid. The ranges specified for such a simulation grid can vary but the following parameters are kept constant unless mentioned otherwise:

- Elevation angle $\theta_e = 45^\circ$.
- Beam width elevation $FWHM_{\theta} = 2.1^{\circ}$.
- Beam width azimuth FWHM_{ϕ} = 2.1°.
- Azimuth simulation grid resolution = 1°, < 1°, 360° >.

The wind velocities within the simulation grid are calculated by Zephyros following the linear wind model (see section 2.3). Other calculation modes of Zephyros are not used during this thesis research. An overview of the first part of the data flow is shown in Figure 3.3. Zephyros calculates various parameters within the simulation grid but only the calculated radial velocity is needed during this research. The result of a generated wind field is shown as PPI in Figure 3.4. Visible is a wind field with two wind layers moving in opposite direction. The PPI is simulated according to the example input grid of Figure 3.2. Due to the elevation angle $\theta_e = 45^\circ$ the PPI represents a conical surface which is typical for radar measurements.

3.3. Noise

The addition of noise to simulated data makes it less synthetic and can be achieved by a random electromagnetic signal added to the original signal. In electronic systems noise is often unwanted but inevitable for most measurement and communication systems. There are various types of noise that vary in their noise power density spectrum like for example white and pink noise. White noise has a constant noise power density for all frequencies while pink noise has a decay in its power density

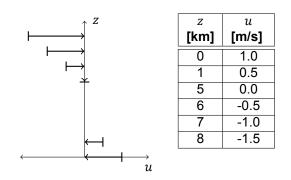


Figure 3.2: Wind profile data used as input for wind field simulation. This wind profile has a lower wind layer from the West and a higher wind layer at a height of 8 km from the East. The values in column z are grid positions and the values for grid positions x and y are zero and thus not shown. The wind speed vectors at that grid positions are given by column u and the values for vectors v and w are zero and thus not shown.

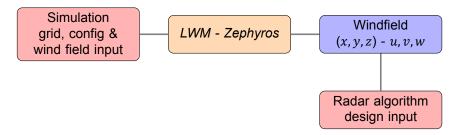


Figure 3.3: Diagram with in and output data needed for radial wind vector determination. The determination of the wind fields is handled by Zephyros.

spectrum for higher frequencies. In the next subsection noise theory is explained first and is followed by an explanation of the used noise model in a separate subsection.

3.3.1. Noise theory

In telecommunications 'Additive White Gaussian Noise' (AWGN) is considered to be a good way to simulate noise onto a signal [16, 18]. A Gaussian is also known to as a Normal distribution and has a variable mean μ and variance σ . Additive white Gaussian noise describes noise that is added to the original signal and has equal uncorrelated powers at all frequencies. The probability density function (PDF) of the Gaussian (Normal) distribution as explained by Taylor [19] is as follows,

$$G_{\mu,\sigma}(x) = \frac{1}{\sigma\sqrt{2\pi}} e^{-\frac{(x-\mu)^2}{2\sigma^2}}.$$
(3.1)

Where:

$G_{\mu,\sigma}$	 Probability density function of a Gaussian 	ı [-] ,
μ	= Mean / expected value (center of the PDF	-) [-] ,
σ	 Variance (width of the PDF) 	[-].

For electronic systems like a radar the thermal noise power caused by attenuating electronic components is defined as,

$$N = kT_s B = kT_s / \tau. \tag{3.2}$$

Where:

Ν	=	Thermal noise power	[W] ,
k	=	Boltzmann constant ($\approx 1,381 \cdot 10^{-23}$)	[J/K],
T_s	=	System Temperature	[K] ,
В	=	Bandwidth	[Hz] ,
τ	=	Pulse length	[s].

Other than the type of noise the signal-to-noise ratio (SNR) is an important characteristic describing

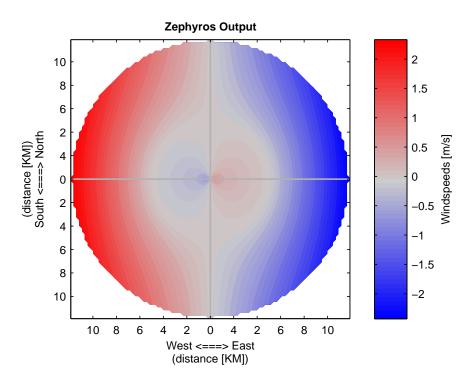


Figure 3.4: Output PPI of a simulated wind field from Zephyros. The used input is shown in Figure 3.2. Wind field is generated for simulation of a radar measuring with a beam width of 2.1°.

the level of noise power compared to the signal power. The SNR is formulated as,

$$SNR = \frac{P_{signal}}{P_{noise}}.$$
(3.3)

SNR	=	Signal-to-Noise Ratio	[W] ,
$P_{\rm signal}$	=	Signal Power	[W] ,
		Noise Power	[W].

The received power of the radar will be lower for ranges further away from the radar, and resulting in a lower SNR for these longer ranges. The radar equation 2.3 can be combined with equation 3.3 to retrieve,

$$SNR = \frac{P_r}{N} = \frac{P_t G_t G_r \sigma \lambda^2 L_s}{(4\pi)^3 r^4 N}.$$
(3.4)

Again note the range dependence of r^{-4} in equation above and see the weather radar equation 2.4 for the r^{-2} range dependence. In radar applications the needed SNR will vary depending on the radar design and techniques applied, but in general a higher SNR will lead to a higher detection ratio Kingsley and Quegan [14].

3.3.2. Noise model

Where:

In order to simulate noise a theoretical noise model is proposed using AWGN with a variable SNR upon users choice. The proposed model determines the Doppler phase θ_d of the simulated velocity v_r with the Doppler ambiguity v_{max} as $\theta_D = \frac{2\pi}{2v_{max}}v_r$. This phase is implemented as a complex signal $(A_d e^{i\theta_d})$ to be added with a complex noise with random phase and Gaussian amplitude. The noise power varies upon range and the r^{-2} dependency is set in combination with the SNR. The SNR is set for a certain range r_0 and is factored with the range r. In short the doppler velocity with noise v'_r and complex noise N_c can be described as follows,

$$v_r' = v_r(\theta_d, A_d) + N_c(\theta_{rnd}, A_{rnd}).$$
(3.5)

And,

$$N_{\rm c}(r) = \frac{1}{\mathrm{SNR} \cdot \frac{r}{r_0}^{-2}} A_{\rm rnd} e^{i\theta_{\rm rnd}}.$$
(3.6)

Where:			
v_r'	=	Doppler velocity with Noise	[m/s] ,
$ heta_{ m d}$	=	Doppler shift	[rad] ,
$A_{\rm dv}$	=	Doppler velocity amplitude	[-] ,
$N_{\rm c}(r)$	=	Noise (range dependent)	[-] ,
r	=	Range	[m] ,
r_0	=	Reference range for specified SNR	[m] ,
A _{rnd}	=	Random Gaussian amplitude	[-] ,
$ heta_{ m rnd}$	=	Random phase	[rad].

3.4. FFWVA - Fast Fourier Wind Vector Algorithm

The Fast Fourier Wind Vector Algorithm (FFWVA) is the name chosen for the horizontal wind determination method. The VAD and DFT are the foundation of the FFWVA method and are combined to retrieve the horizontal wind speed and direction. This section focuses on the operation of the FFWVA method. The VAD was already explained in section 2.4. In the first subsection an explanation of the frequency domain is given. This is followed by a subsection covering the the DFT theory and the FFT algorithms calculating this in Matlab.

The last three subsections will cover a DFT calculation example. The example uses the azimuthal (round) scan and Doppler velocity data from an earlier example. This example is used for explanation of the horizontal wind determination after the DFT. The wind direction determination is determined through the found DFT phase and the wind speed though the found DFT amplitude. An overview of the complete simulation set up including the proposed FFWVA method is shown in Figure 3.5. Visible is that the FFWVA method uses the simulated wind field velocities of Zephyros as input, and simulating velocities as if retrieved from a Doppler radar.

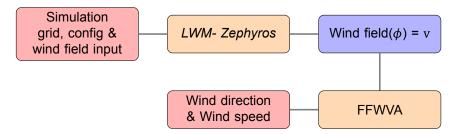


Figure 3.5: Diagram of Zephyros simulation set up with wind direction and speed estimation through the FFWVA. Compared to Figure 3.3, wind field (x, y, z) - u, v, w is used in polar form.

3.4.1. Frequency domain

Signals in the frequency domain are described with the amplitude and phase for a certain frequency, but in time domain the signal is described with an amplitude at a specific moment in time. The frequency domain helps to find, describe, measure and analyse the 'contents' of signals as it exposes the various frequencies a signal is built off. These frequencies are electromagnetic waves like the waves surrounding us: light, data communications signal, radar signals, etc. A visual representation of the time vs. frequency domain is shown in Figure 3.6, it shows identical information in time and frequency domain. Visible is that the frequency domain needs less data for the description of the existing frequencies but time information of the start and end of the frequencies is lost.

Analyzing, modification and storage of electromagnetic signals in the frequency domain is very common in digital systems. Signals in the frequency domain can be mapped back to the time domain for use in the physical world. This move is mathematical and called a transformation. There are various transformations available like the well-known Fourier transform [20]. The various transforms available vary in mapping from and to the frequency domain. The Fourier transform mapping is a

linear mapping to a complex number. The loss of time information is a limitation but can sometimes be overcome with other transforms like the short-time Fourier transform. A benefit of the DFT in digital system is storage of (electromagnetic) wave information while gaining computational benefits. The DFT is further explained in the next section.

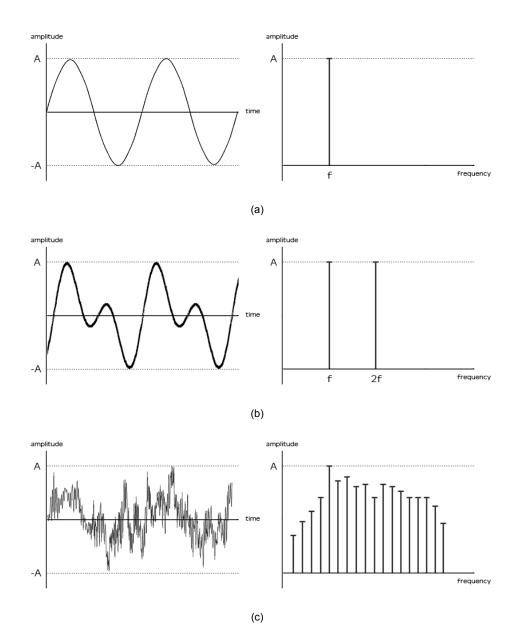


Figure 3.6: Overview of time domain versus frequency domain. In Figure (a) a single frequency is represented on the left in time domain and in frequency domain is represented on the right. Figure (b) is identical to (a) but with an extra harmonic visible. Figure (c) shows a multiple of frequencies. The signal has a noise like shape. *Note: Image from http://www.erzetichaudio.com.*

3.4.2. Discrete Fourier Transform

The Fourier transform is a method that transforms functions from the time domain to the theoretical frequency domain. As explained in the previous subsection (3.4.1) the Fourier transform describes amplitudes and phases of researched harmonic frequencies. It will be used during the development of the proposed analysis method for horizontal wind speed determination. The Fourier and inverse

Fourier transform are written as follows,

$$X(\omega) = \frac{1}{\sqrt{2\pi}} \int_{-\infty}^{\infty} x(t) \cdot e^{-i\omega t} dt, \qquad (3.7)$$

$$x(t) = \frac{1}{\sqrt{2\pi}} \int_{-\infty}^{\infty} X(\omega) \cdot e^{i\omega t} dt.$$
 (3.8)

Where:

$X(\omega)$	=	Frequency spectrum (complex function)	[-] ,
x(t)	=	Signal as function of time	[-] ,
ω	=	Angular frequency ($\omega = 2\pi f$)	[rad/s] ,
t	=	Time	[s].

These are continues transforms mainly usable for analytical purposes. They are rewritten for a discrete approach usable for sampled signals and as bridge between the real and digital world. For sampled signals the discrete variants of the Fourier transform is reformulated as,

$$X_k = \sum_{n=0}^{N-1} x_n \cdot e^{-i2\pi k n/N},$$
(3.9)

$$x_n = \frac{1}{N} \sum_{k=0}^{N-1} X_k \cdot e^{i2\pi kn/N}.$$
(3.10)

Where:

X_k	 Number of frequencies 'k' (complex) 	[-] ,
x_n	= Signal at point 'n'	[-] ,
N	 Number of samples (DFT window size) 	[-] ,
п	 Considered sample position 	[-] ,
k	 Considered frequency 	[-].

The above discrete Fourier transform is discrete in both time and frequency domain. The resolution of the resulting DFT (the bin size) depends on the sample frequency f_s of the original signal x_n and chosen number of DFT samples *N*. The number of DFT samples *N* is also known as the DFT window. The DFT bin size (spectral frequency resolution) is described as,

$$\Delta f = \frac{f_s}{N}.\tag{3.11}$$

Where:

Δf	=	DFT bin size (frequency resolution)	[-] ,
f_s	=	Sample frequency	[-].

Until this point the sample frequency is referred to per time unit (1/t), and is useful when sampling a sine in time domain. However it can also represent less straightforward units like an angular unit (1/rad) as will be used during this research.

Choosing the correct bin size (DFT window) is of great essence as it can help to minimize DFT artefacts, e.g. spectral leakage and an unnecessary large time resolution. The time resolution artefact exists when a large DFT window is chosen, and in that case a higher sample frequency or a larger sample period is required. Spectral leakage is visible as side lobes in the frequency spectrum and also as an inaccurate amplitude determination. For the suppression of side lobes windowing techniques are helpful and help to improve the amplitude determination accuracy. If the focus lies on accurate amplitude determination zero padding will also provide improved amplitude determination (main lobe). With the zero padding technique the frequency resolution (smaller bin size) increases without requiring a larger DFT sample window and can help to align frequencies bins [16, 21].

In order to optimize the DFT and calculate it in a more efficient manner the fast Fourier transform (FFT) will be discussed. In general the FFT is an algorithm that calculates the DFT in a more efficient manner, but with a resulting output that is identical to the normal DFT. Most FFT algorithms do have a

restriction on the size of the input known as the DFT window. For example a well-known FFT algorithm of Cooley and Tukey [22] is only applicable if N is a power of 2 ($N = 2^n$). In their algorithm optimization is achieved through recursion with N split in odd and even values. The recursion symmetry between the odd and even parts is exploited by most FFT algorithms leading to less computations compared to the DFT [4, 23, 24].

In comparison if the DFT is calculated without further optimizations as shown in equation 3.10 it needs $\Theta(N^2)$ operations. Where the FFT algorithms are calculated within $O(N \log_2 N)$ operations which is significantly less [22]. The notations of operation complexity are referred to as the Big O notation. In the Big O notation the Θ represents a tight bound which is both and upper and a lower bound and the O is an upper bound.

In Matlab the calculation of DFT's is handled by the FFTW library which contains various FFT algorithms. An important aspect of the FFTW library is that it can calculate DFT's of arbitrary size, thus without the N² requirement, within $O(N \log_2 N)$ operations. The FFTW library achieves this with a combination of various algorithms and a planner. The planner calculates an optimal path, with the appropriate algorithms, the first time a new arbitrary size DFT is calculated [25]. Due to this freedom where the FFTW library can calculate arbitrary sized DFT's with relatively low amount of operations, and this can also be used to optimize the bin size (DFT window).

3.4.3. Discrete Fourier Analysis of the Velocity Azimuth Display

The proposed method uses a single round scan from a (simulated) wind field retrieval as input of a DFT to determine the wind speed and direction. As mentioned earlier the velocities of a single round scan can be displayed with the measured velocities plotted to the azimuth. An example of this was given earlier and is shown again in Figure 3.7. The plotted data has a sinusoidal shape represented by $y = 20 \sin(2\pi t)$. The VAD is a frequency based analysis method as it determines the horizontal wind parameters with a Fourier series, while the proposed FFWVA method is similar the difference is that the DFT is used. The plotted data is sampled discretely and is transformed to the frequency domain with the discrete Fourier transform. The output of the DFT are frequency bins but do not relate to a physical frequency.

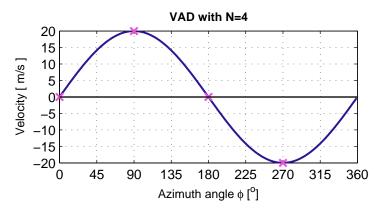


Figure 3.7: Velocity data plotted to the azimuth of a simulated radial wind speed of 20 m/s from the West to the East. Four samples (N=4) are indicated that are used as input for a DFT calculation example.

In order to get a better idea of the proposed FFWVA method and its analysis in the frequency domain an example calculation is discussed. Consider the sinusoidal period of the VAD example shown earlier plotted again Figure 3.7. Four indicated sample points (N=4) are added and are also visible in that plot. In radians the period begins at 0 rad (0°) and ends at 2π rad (360°). The sampled signal can be described as function $x_m = 20 \sin(2\pi m/N)$. Here *N* is the total number of samples and *m* is the sample interval number. This notation is helpful for the DFT of x_m which now can be written

as,

$$c_{k} = \sum_{m=0}^{N-1} x_{m} \exp(-2\pi i \frac{mk}{N}) (k = 0 : N - 1),$$

$$c_{k} = \sum_{m=0}^{N-1} 20 \sin(\frac{2\pi m}{N}) \exp(-2\pi i \frac{mk}{N}) (k = 0 : N - 1).$$
(3.12)

Equation 3.12 can also be written in matrix form. With four samples (N = 4) and substitute $W = \exp(-\pi i/2)$ the result is as follows,

$$\begin{pmatrix} c_0 \\ c_1 \\ c_2 \\ c_3 \end{pmatrix} = \begin{pmatrix} 0 \\ 20 \\ 0 \\ -20 \end{pmatrix} \begin{pmatrix} 1 & 1 & 1 & 1 \\ 1 & W & W^2 & W^3 \\ 1 & W^2 & W^4 & W^6 \\ 1 & W^3 & W^6 & W^9 \end{pmatrix} = \begin{pmatrix} 0 \\ -40i \\ 0 \\ 40i \end{pmatrix}.$$
(3.13)

The found (complex) values of the DFT are the phases and amplitudes at their representing frequencies. The four calculated c_k values are known as the DFT frequency bins and their representing frequencies are $f = f_0 * k$ (i.e. 0,1,2 & 3 Hz). For real inputs the frequency bins larger than N/2 + 1 are considered redundant, and are often shifted for a better visualization as can be seen in Figure 3.8(a). Due to this redundancy only two data points are useful of this N = 4 example. The remaining two data points are plotted in Figure 3.8(b). The shown values in these plots are normalized and do not visualize the found phase information. The normalization of the DFT is explained and used as example in subsection 3.4.5. The phase angle θ at a certain frequency is found with use of the real and imaginary parts as $\theta = \arctan(b/a)$. The amplitude or DFT power for a specific frequency is found with $P_{dft} = |\sqrt{a^2 + ib^2}|$.

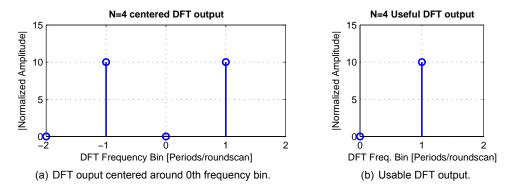


Figure 3.8: DFT output of a single round scan example with 4 inputs as shown in Figure 3.7. On the left (a) the centered FFT is shown and on the right (b) the two useful data points are shown. The direction (phase information) of the wind is not readable from this amplitude plot.

The '0'th frequency bin is called the DC component as is will represent a fixed offset in the data. The first harmonic bin of the DFT is used by the FFWVA for the needed DFT power and angle as described by the VAD method. This idea is identical to the VAD as it also uses the first harmonic of the Fourier series. To further explain the determination of the radial wind direction and speed this example is used further in the next sections. From the found DFT phase an estimation for the direction of the wind can be made, and the determined DFT amplitude makes estimation of the wind speeds possible.

3.4.4. Determination of the Wind Direction after DFT

In time domain finding the maximum velocity at a certain range represents the direction of the wind at the found angle. After the DFT calculation the phase of the first DFT harmonic corresponds to the

wind direction and is described as,

$$a + bi = DFT(V(\phi)) \qquad (\phi = 0: 2\pi),$$

$$\Theta = \arctan(b/a) \qquad (-\pi/2 \le \Theta \le \pi/2),$$

$$\phi_{wd} = -\arctan(b/a) + \pi \qquad (0 \le \phi_{wd} \le 2\pi).$$
(3.14)

In the formula above the last line helps to find the wind direction values ϕ_{wd} as introduced and defined in the Table 3.1. As with the VAD method arctan can be replaced with the function atan2. The atan2 function solves the discontinuities of the arctan and outputs the correct quadrant. The found wind direction of the example DFT calculation can be determined as $-atan2(-40, 0) + \pi = 270^{\circ}$. In this determination a = -40 and b = 0 and the results corresponds with the Westerly wind. As a second example the previously generated wind field shown in Figure 3.4 will be used as input. Because every round scan represents a certain distance from the radar the determined wind directions can vary for different distances from the radar. The determined wind directions for the second example are visible on the left hand side of Figure 3.9. Visible from these examples is this that the proposed FFWVA is able to use the DFT to retrieve the horizontal wind direction successfully in a straight forward manner.

3.4.5. Determination of the Wind Speed after DFT

As the wind direction is successfully determined after the DFT is calculated the next step is the horizontal wind speed determination. The amplitude of the first frequency bin of the DFT output will represent the wind speed of the radial velocity round scan input. Normalization by division of the DFT power with the number of data points (N) allows for retrieval of the correct winds speeds. The horizontal wind speed can be determined as follows,

DFT
$$(V(\phi)) = a + bi$$
 $(\phi = 0 : 2\pi),$
 $|\sqrt{a^2 + b^2 i}| = P_{dft},$
 $v'_h = \frac{2P_{DFT}}{N}$ (radial),
 $v_h = \frac{2P_{DFT}}{N} / \cos(\alpha).$
(3.15)

The found radial velocity v'_h is the amplitude of the example sine and thus corresponds with the wind speed. Dividing the measured radial velocity by the cosine of the elevation angle α retrieves the horizontal speed v_h . The power is multiplied by two due to the redundant part of the real DFT. Applying this on the DFT calculation example the found radial wind speed is $2\sqrt{(-40)^2}/4 = 20$ m/s. The results of the second example with the complete wind field of Figure 3.4 is visible on right hand side of Figure 3.9. Visible is that the FFWVA is able to use the DFT to retrieve the wind speed successfully just like the wind direction in the previous section.

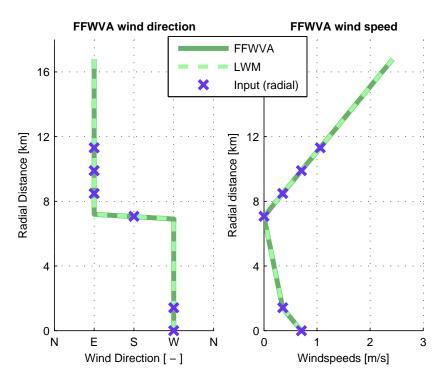
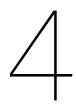


Figure 3.9: Plotted are the determined wind direction and speed determined by the FFWVA method and the LWM method. As reference the wind profile input is plotted, the input points shown are the radial projection and thus vary from the wind profile input of Figure 3.2.



Results

In this chapter the proposed FFWVA horizontal wind estimation method is tested in various scenarios, and a comparison is made to the linear wind model. As explained in section 3.4 the FFWVA uses the radial velocities from a single azimuthal round scan as input. The radial velocities are retrieved from wind field simulations handled by Zephyros. These simulations of wind fields are performed with a specified wind profile as input. Next sections will cover results of both methods in the following cases:

- Simulated wind fields.
- · Simulated wind field with addition of noise.
- Simulated wind field with missing, gapped, data.
- Measured Doppler radar data.

These simulation scenarios are chosen for an operation verification of the FFWVA method. The results of these tests are reviewed to make a comparisons with the LWM and indicate the performance of the FFWVA.

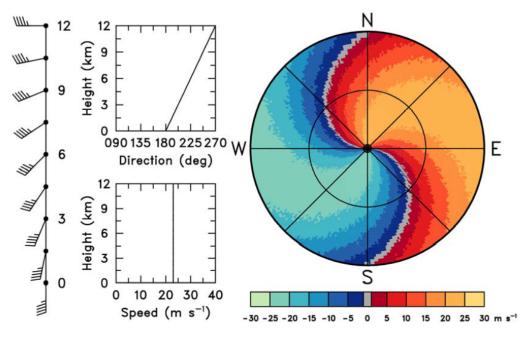
4.1. Simulations

The first simulations are performed on wind fields with known wind profiles as described in the Doppler interpretation guide of Brown and Wood [13]. From that Doppler interpretation guide two wind profiles are selected and used as input wind profile. Both wind profiles have a double wind layer from various directions. The double wind layer is chosen to test the methods on a multi-layered wind field as explained in section 2.1. The resulting simulated wind field is compared with the information found in the Doppler interpretation guide. The output of the FFWVA form the retrieved wind profile, and show the determined wind speed and wind direction. Ideally the wind profiles used as input for the simulation will correspond to the output results of the FFWVA.

4.1.1. Double Layered Wind Profile with Gradual Transition

The first simulated wind field consist of two layers of wind with a gradual transition in direction and a constant wind speed.

The transition is reproduced from the Doppler interpretation guide of Brown and Wood [13] and is shown in Figure 4.1. Visible is a lower southern wind wind layer and a higher wind layer that originates from the west (a double layered wind field). In order to simulate this with Zephyros a wind profile is needed, and the used simulation input is shown Figure 4.2. Note that data given in the table of that figure is shaped with help of goniometric functions. The resulting simulation is a wind field as measured by Doppler radar and is displayed in Figure 4.3. This figure shows the simulated Doppler velocities for the various azimuthal round scans. When applying the FFWVA and the LWM methods the wind speed and wind direction are determined, and this results is plotted in Figure 4.4. Visible is that the determined wind direction and wind speed are identical to the input wind profile, and this is also plotted in the same figure. In this case, with two wind layers from different directions and a



gradual transition between them, the result is that the proposed FFWVA and LWM perform similar and retrieve the horizontal wind speed and direction correctly.

Figure 4.1: Doppler interpretation by Brown and Wood [13] of a double layered wind profile: a lower southern wind and a higher western wind with a gradual transition between them.

$\uparrow Z$	$\uparrow Z$	Ζ	и	ν
		[km]	[m/s]	[m/s]
		0	$sin(\pi(0/12))$	$\cos(\pi(0/12))$
		2000	$sin(\pi(1/12))$	$\cos(\pi(1/12))$
		4000	$sin(\pi(2/12))$	$\cos(\pi(2/12))$
, ' ←	 , 1 , 4 	6000	$sin(\pi(3/12))$	$\cos(\pi(3/12))$
 ⊢ ⊢ 	⊷	8000	$sin(\pi(4/12))$	$\cos(\pi(4/12))$
н	· · ·	10000	$sin(\pi(5/12))$	$\cos(\pi(5/12))$
\checkmark \longrightarrow	$ \longleftrightarrow $	12000	$sin(\pi(6/12))$	$\cos(\pi(6/12))$
u	v			

Figure 4.2: Wind profile used as input for the simulation of a double layered wind profile with gradual transition. In the table z is a grid positions, grid positions x and y are zero and are thus not shown. The wind velocity vectors specified at that grid position are u and v, vector w is zero and are thus not shown.

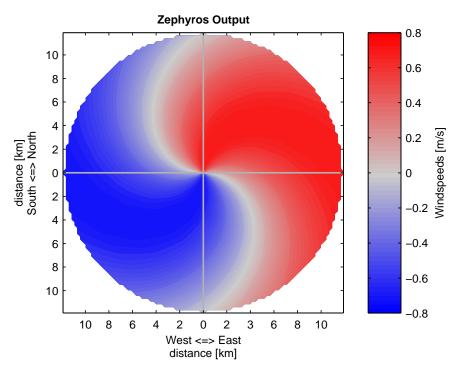


Figure 4.3: Wind simulation output of a double layered wind profile with a gradual transition. The defined wind profile used as input for this simulation is given in Figure 4.2.

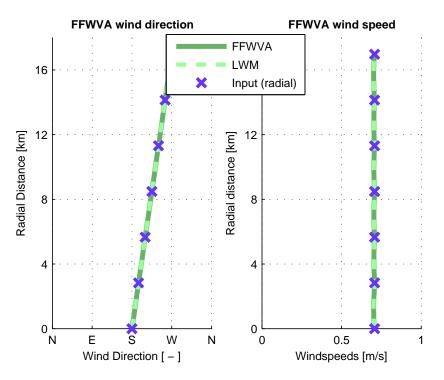


Figure 4.4: Output of the FFWVA method displaying the determined horizontal wind field parameters. The results of the LWM and radial input data points are plotted for comparison and as a reference.

4.1.2. Double Layered Wind Profile with a Discontinuity

In this section a second wind field is simulated, again with two layers of wind from different directions, but with hard transition in between them (a discontinuity). This hard transition is also reproduced from the Doppler interpretation guide of Brown and Wood [13] as visible in Figure 4.5. The used wind profiles and table with data points used as input for this simulation are shown in Figure 4.6. These data points are also shaped with help of a goniometric function just like the previous wind field. The resulting wind field has a lower eastern wind and a higher western wind (double layered wind field). The simulated Doppler velocities are displayed in Figure 4.7. Doppler velocities from the simulation are the input for the FFWVA and LWM methods. Horizontal wind field retrieved by the methods are plotted in Figure 4.8. In the Figure the radial input data points are also visible as a reference. In this second case, with two wind layers and a hard transition, both the FFWVA and LWM perform similar and retrieve the horizontal wind speed and direction are determined correctly again.

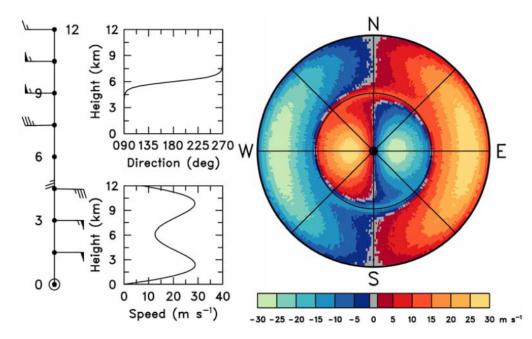


Figure 4.5: Doppler interpretation by Brown and Wood [13] of a double layered wind profile with discontinuity at height = 6 km.

$\uparrow Z$	$\uparrow Z$	Z	u	v
		[km]	[m/s]	[m/s]
		0	$sin(-2\pi(0/12))$	0.0
	Ţ	2000	$sin(-2\pi(2/12))$	0.0
	$\overline{\mathbf{x}}$	4000	$sin(-2\pi(4/12))$	0.0
× '	$\leftarrow 1$	6000	$\sin(-2\pi(6/12))$	0.3
\longmapsto	¥ '	8000	$sin(-2\pi(8/12))$	0.0
>	¥	10000	$\sin(-2\pi(10/12))$	0.0
$\leftarrow $	\downarrow \rightarrow	12000	$\sin(-2\pi(12/12))$	0.0
	u v			

Figure 4.6: Wind profile input used for simulation of a double layered wind field with hard transition (discontinuity). Only grid position z is shown, grid positions x and y are zero and are thus not shown. The specified velocity vectors at that grid position are u and v, vector w is zero and is thus not shown.

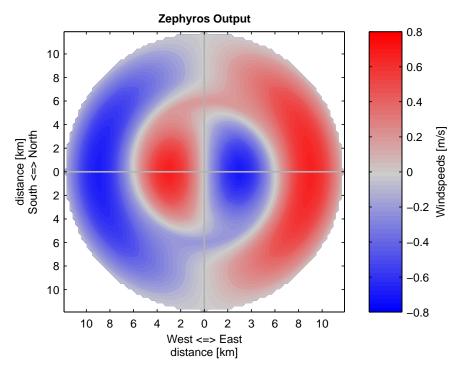


Figure 4.7: Results of the wind simulator output of double layered wind profile with gradual transition. The defined input wind profile used to perform this simulation is shown in Figure 4.6.

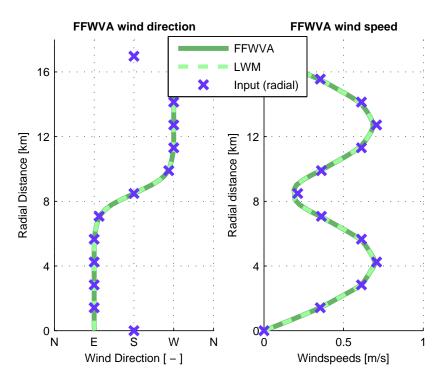


Figure 4.8: Output of the FFWVA method displaying the determined horizontal wind field parameters. The results of the LWM and radial input data points are plotted for comparison and as a reference.

4.2. Simulation with Noise

The next step in expanding the simulation scope is the addition of noise with different SNR levels. The chosen wind field for the additional simulations is the double layered wind field with hard transition (discontinuity) as seen in the previous section (4.1.2). Other than the noise all other parameters are kept identical to the previous section. The addition of noise is simulated by lowering the SNR to 13, 8 and 0 dB with the model proposed in section 3.2. Before application of noise onto the simulation the results of the proposed model are first reviewed in the next subsection.

4.2.1. Noise model results

Before application of the noise simulation model, the noise output is tested with and without the range dependency. Histograms of these results are visible in Figure 4.9 and Figure 4.11. In Figure 4.9 the histogram of the modelled noise without range dependency is visible. The range dependency is removed by setting a fixed range $(r = r_0)$ resulting in noise with the same power for all ranges. In Figure 4.11 the results are visible with range dependency, and effectively generating noise with a lower power for less distant ranges. Visible is that the noise model has a Gaussian distribution with variance = 0.013 m/s and standard deviation = 0.11 m/s. These low values explain the relatively small peak of the distribution. Without the range dependence the variance and standard deviation are even smaller: 0.0032 m/s and 0.057 m/s respectively. These lower values are as expected because the noise power for less distant ranges is lower. The result is a larger sum of noise with low noise powers near zero. Noise with a lower noise power has more values near zero resulting in a less wide, but higher shaped histogram compared to the histogram without range dependence. In Figure 4.10 and 4.12 examples of generated noise are plotted for a complete range bin at a fixed azimuth direction. Visible is that Figure 4.10 has an equal noise power for all ranges. Figure 4.12 has no noise for near distances and an increasing noise power for larger distances. These figure's show that the noise model works as expected: with a Gaussian shaped histogram and increasing noise power for larger ranges.

4.2.2. Wind determination from data with noise.

The performance of the FFWVA is tested further with the SNR simulated at various noise levels. In Figure 4.14 the noise is simulated at a SNR level of 13 dB without range dependence. Noise with a range dependency is simulated with SNR's 8 and 0 dB at 16 km. The results of these simulations are visible in Figure 4.16 and 4.18 respectively. Visible in the results is that for these three simulated SNR levels both the FFWVA and the LWM methods determine the wind direction correctly. The determined errors of in the wind speed and direction determination are available in Table 4.1. Visible is that the LWM and FFWVA both have identical average errors. This full coverage noise test, with an signal-to-noise ratio lowered to SNR = 0 dB at 16 km, the FFWVA determines the wind speed and wind direction correctly.

SNR	Avg. direction error		Avg. speed error		
[dB]	LWM [°]	FFWVA [°]	LWM [m/s]	FFWVA [m/s]	
13	1.05	1.05	0.01	0.01	
8	1.66	1.66	0.01	0.01	
0	12.05	12.05	0.09	0.09	

Table 4.1: The average errors in the determination of the wind speed and wind direction.

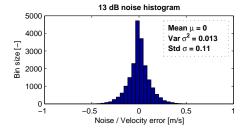


Figure 4.9: Histogram of noise distribution without range dependency (fixed range $r = r_0$).

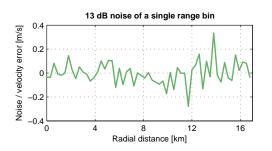


Figure 4.10: Noise error of a single range bin without range dependency (fixed range $r = r_0$).

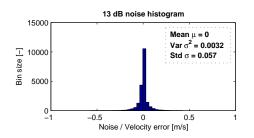


Figure 4.11: Histogram of noise distribution with range dependency.

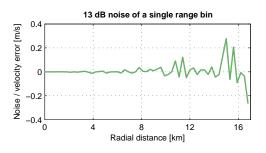


Figure 4.12: Noise error of a single range bin with range dependency.

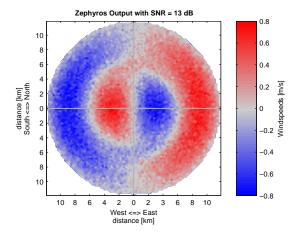


Figure 4.13: Wind field simulation with SNR = 13 dB, without range dependency. Other parameters identical to Figure 4.6.

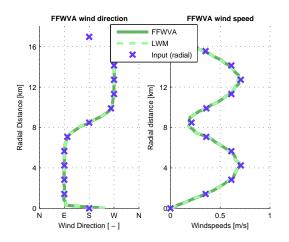


Figure 4.14: Wind direction and wind speed determined by FFWVA and LWM on wind field with SNR = 13 dB as shown on left.

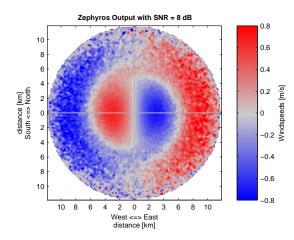


Figure 4.15: Wind field simulation with SNR = 8 dB at 16 km. Other parameters identical to Figure 4.6.

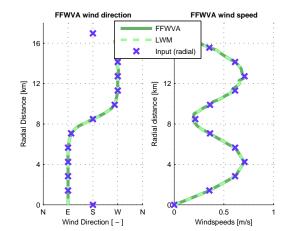


Figure 4.16: Wind direction and wind speed determined by FFWVA and LWM on wind field with SNR = 8 dB at 16 km as shown on left.

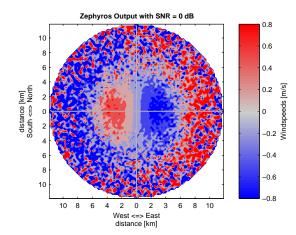


Figure 4.17: Wind field simulation with SNR = 0 dB at 16 km. Other parameters identical to Figure 4.6.

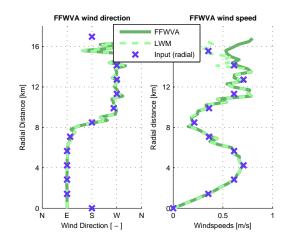


Figure 4.18: Wind direction and wind speed determined by FFWVA and LWM on wind field with SNR = 0 dB at 16 km as shown on left.

4.3. Simulation with Gapped Data

The last simulation step is the addition of gaps in the simulated wind field data. The simulation of gaps is interesting because missing data is very likely in a real radar measurement. There are multiple reasons a radar retrieval will miss data like the detection of clutter (unwanted echoes) or simply no echo. For the simulation of gaps the same double layered wind field with hard transition as seen in section 4.1.2 is used. Two types of gap simulations will be discussed: a single continuous gap and multiple reoccurring gaps with an even spread. The gaps are simulated by setting the radial velocity equal to zero where the gap is simulated.

4.3.1. Single continuous Gap

A single continuous gap is a simulation where one chunk of the simulated velocity data is set to zero. The result of the simulation with a single gap, starting at azimuth $\theta = 180^{\circ}$ and a size gap of 108° (30%), is visible in Figure 4.20. As an example a single round scan from this simulation, with single gap from starting position $\theta = 180^{\circ}$, is plotted in Figure 4.19. Two FFWVA results are available in that plot: with and without normalization. This extra FFWVA normalization is performed on the wind speed determination (the DFT amplitude) as an underestimation is made due to the missing data of the gap. The extra normalization is performed as $v_h/(1 - \text{gapsize})$ effectively normalizing for the remaining data points, and is in addition to the DFT normalization explained in section 3.4.5. The results of the horizontal wind determination with this single gap are plotted in Figure 4.21. The results without gap normalization is plotted as a reference, but will be left out for other gapped results. Visible is that the single gap simulation with zero's results in an error of the determined wind direction and an error in the determined wind speed.

To further analyze the single gap behavior the DFT is calculated on velocity data of a single round scan as the FFWVA proposes. Additionally varying the gaps size and simulate various gap starting positions. The simulated gap sizes range from 0° to 270°, 0% to 75% gaps. The gap starting position is simulated by varying the phase of the DFT input which in case of the FFWVA represents the wind direction. Varying the wind direction (input phase) with fixed gap position versus varying the gap starting position gives comparable results considering the error over the entire domain < 0, 2π >. The determined average errors are shown in Figures 4.23 and 4.22 with the determined phase error and determined amplitude error respectively. These errors in wind speed are also normalized with the gap size and shows error up to 60% at gap size 270°(75%) for specific phases. The errors in wind direction are up to 40° at 270°(75%) gap size which is an error of approximately 11%. This simulation visualizes how the phase and amplitude error do not rise in a constant matter and vary upon the input data. The following observations are made:

- For gap sizes from 0° to 180° the amplitude error remains lower than 25% and the phase error lower than ±15°(≈ 5%).
- For a gap size $\approx 180^{\circ}$ there seems to be an optimum and the errors are relatively low.
- For gap sizes larger than 180° to the tested 270° the errors rise to an amplitude error of 60% and a $\pm 40^{\circ}$ error in phase.

The observation with a gap size of 180° is interesting as it can be exploited for cases where more data is available. The gap simulation results show that the FFWVA is able to determine the horizontal wind parameters with an extra normalization, but wind speed and wind direction errors vary upon gap size and gap starting position.

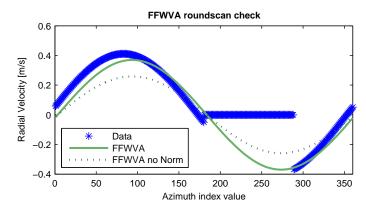


Figure 4.19: Velocity data plotted to the azimuth of a single round scan with gap. The data is set to zero at gap position.

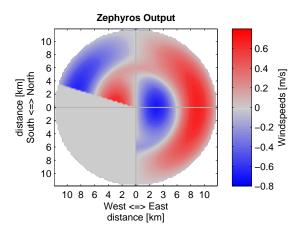


Figure 4.20: Example of simulation with 30% gap (108°) and 50% (180°) azimuth starting point. Other than the gap it's identical to Figure 4.7.

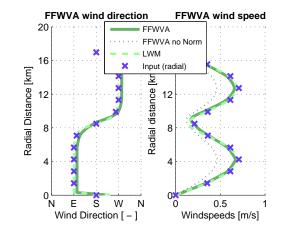
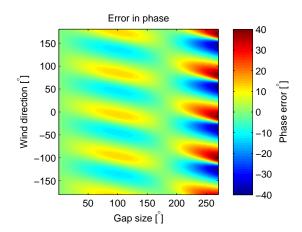


Figure 4.21: Output of the FFWVA and LWM displaying the determined wind direction and the determined wind speed with gap in data.



Error in amplitude 60 150 40 100 Amplitude error [%] Wind direction [[°]] 20 50 0 0 -50 -20 -100 40 -150 -60 50 100 150 200 250 Gap size []

Figure 4.22: DFT amplitude error output as simulation of radial velocity input signal with increasing gap and variable wind azimuth direction.

Figure 4.23: DFT phase error output as simulation of radial velocity input signal with increasing gap and variable wind azimuth direction.

4.3.2. Multiple reoccurring gaps

Other than a single gap, the simulation of smaller reoccurring gaps with an even spread in the azimuth direction is of high interested because of its periodicity. Comparable periodicity is present in the sum used applying the VAD method. The sum is part of the Fourier series over the domain $< 0, 2\pi >$. The simulation of a first example with reoccurring gaps is available in Figure 4.24. Visible are six evenly spread gaps with an equal amount of velocity data. The results of the horizontal wind determination methods are plotted in Figure 4.25. Comparing the results to the input wind profile the average error in wind direction determination of the FFWVA is negligible and the average error of the LWM is approximately 2.56°. Without normalization the wind speed determination is half of the expected value due to the exact 50% data coverage. With normalization for the gaps applied the wind speed determination is as expected and with negligible error.

The horizontal wind determination through the FFWVA show comparable results when varying the simulations with: less data compared to the gaps, various starting positions and/or the addition of noise. A second simulation example with reoccurring gap is shown in Figure 4.26. This second example has five evenly spread gaps with noise set at SNR 8 dB with range dependency. The gaps have an offset in the starting position (start with data instead of gap) and the simulated gaps are larger compared to the remaining velocity data. The results of the horizontal wind determinations are shown in Figure 4.27. Visible is that wind direction determination is correct with both methods. Compared to the input wind profile the average error in wind direction determination of the FFWVA is 3.84° and the average error of the LWM is approximately 5.42°. With periodic, evenly spread, gaps the wind direction determination of the FFWVA.

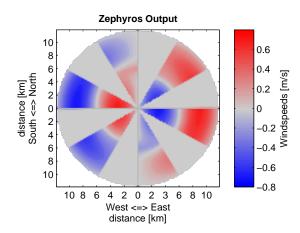


Figure 4.24: Simulation with hard transition of a double wind layer profile and six evenly spread reoccurring gaps. Other than gap this simulation is identical to Figure 4.7.

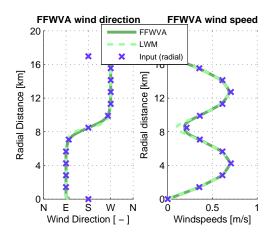


Figure 4.25: Output of the FFWVA and LWM displaying the determined wind direction and the determined wind speed obtained with the reoccurring gaps in the data. The average error in the wind direction is < 0.01° for the FFWVA and $\pm 2.56^{\circ}$ for the LWM.

4.4. Real data from X-Band Weather Radar

In order to enhance testing of the FFWVA method it is tested on real measurement dataset from a X-Band Doppler radar of Thales positioned in Toulouse. The tested data is made available in the UFO project that has partners like KNMI, Thales, TU Delft and others. The used dataset is characterized by a gap with missing data caused by a part that could is not scanned due to regulations of the nearby Toulouse-Blagnac airport. Other than that gap the data has good coverage with a determined Doppler velocity from other directions without other gaps. This radar measures with an azimuth and elevation resolution of $\approx 1.7^{\circ}$ and a range resolution of 108 meters. The minimum and maximum ambiguous ranges are approximately 4 and 40 km respectively. The dataset contains measurements at elevation angles $\theta \approx 3.5^{\circ}$, $\theta \approx 5.0^{\circ}$ and $\theta \approx 6.5^{\circ}$. The used radar data is available in Figure 4.28) at elevation angle $\theta \approx 6.5^{\circ}$, the data was measured around half past two in the afternoon on 24st of April-2014. The results of the FFWVA and LWM are plotted in Figure 4.29, the results indicates a Northerly wind with a wind speed of approximately 7 m/s. Various historical weather data websites like

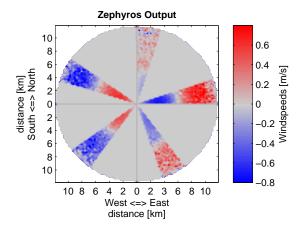


Figure 4.26: Simulation with hard transition of a double wind layer profile and five evenly spread reoccurring gaps with noise. Other than gap this simulation is identical to Figure 4.7.

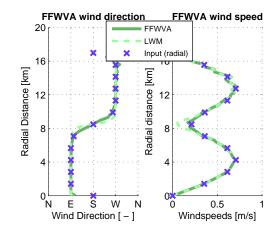


Figure 4.27: Output of the FFWVA and LWM displaying the determined wind direction and the determined wind speed obtained with the reoccurring gaps in the data. The average error in the wind direction is $\pm 3.84^{\circ}$ for the FFWVA and $\pm 5.42^{\circ}$ for the LWM.

timeanddate.com and eurometeo.com verify that a Westerly to North-Westerly wind was measured at that time and date in Toulouse. Compared to the PPI the wind speed determination seems correct, but a normalization for the gap with missing data was needed. The gap size needed the gap normalization was retrieved from the azimuth information this in comparison to the determination of gap size through the found zeros with the simulations. The horizontal wind determination of the LWM and FFWVA methods are comparable in this tested data set.

4.5. Processing Time

The processing times of the FFWVA and LWM are compared to have a benchmark other than the output error. The results of first thousand iterations of 5000 are plotted in Figure 4.30. The shown iterations are for a single round scan with 360 Doppler velocities from every azimuth degree as input for the determination of the wind speed and wind direction. The determined averages are:

- Average processing time for the FFWVA per round scan is 110 ms (0.0110 s).
- Average processing time for the LWM per round scan is 334 ms (0.0334 s).

The individual iteration times are determined with the tic tac time commando's run in Matlab 2014a on an Intel Core i5-M560. Variations with gaps and/or noise have no influence on the determined averages as the amount of data stays constant. These results show that the FFT function of Matlab seems to be processed in a faster manner compared the lsqlin function of Matlab.

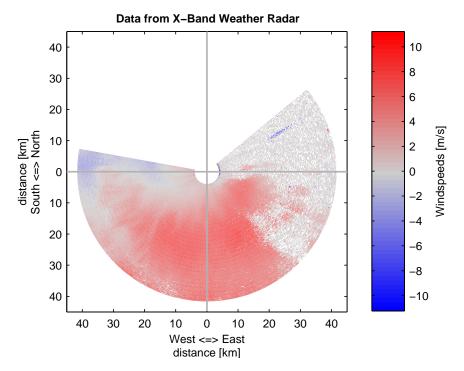


Figure 4.28: Data from X-band weather radar of Thales. Measured on 24-04-2014 at an elevation of 6.5° and with a beam width of approx. 1.7°.

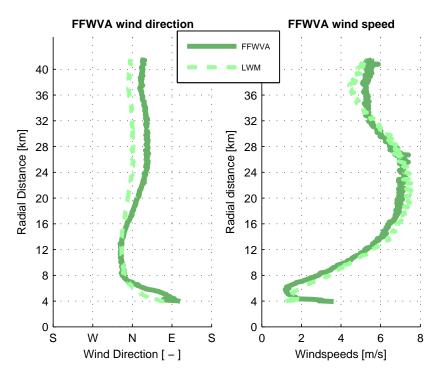


Figure 4.29: Output of the Fourier analysis displaying the determined wind direction and the determined wind speed of the X-band weather data of figure 4.28. The results of the LWM are plotted as a reference.

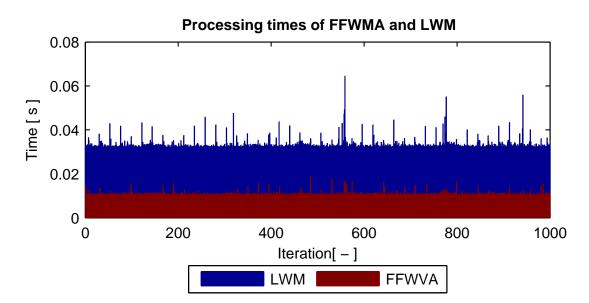


Figure 4.30: Processing times of the first thousand iterations to determine average processing times.

5

Conclusion & Recommendations

As last part of this thesis research this chapter will cover the results of the FFWVA, the conclusions and the recommendations. The performance of the proposed frequency based wind retrieval method named the Fast Fourier Wind Vector Algorithm (FFWVA) is compared to the linear wind model (LWM). All results of this comparison are reviewed in the first section. Out of these results the conclusion will be drawn in the section afterwards. The last section will address the recommendations for future work as finalization of this research.

5.1. Summery of Results

Different scenarios are simulated in order to review the FFWVA's performance with more realistic conditions. A comparison with a common method the LWM is available throughout this thesis with the various results. Other than ideal conditions, with full coverage and no noise, noise and data gaps are both simulated.

In the ideal case with full coverage and no noise both the LWM and FFWVA retrieve the correct wind direction and speed. The wind direction and speed are determined with negligible error with both the LWM and the FFWVA method. This shows that the FFWVA method is functioning fundamentally as a horizontal wind retrieval method.

Noise with a range dependency is added to the simulation with a SNR as low as 0 dB at 16 km, and the FFWVA and LWM remain to perform with identical error at this SNR level.

When simulating with a single gap smaller than 50% in the azimuthal velocity data the FFWVA is still able to retrieve the horizontal wind parameters, but with an error up to 20% for the wind direction and up to 5% for the wind speed determination. In this case with a single gap the LWM performs better than the FFWVA as it has a lower error for most gap sizes.

An optimum is found with a gap of exactly 50% data with an identical low error in the horizontal wind parameters compared to the LWM.

In a scenario with multiple equally spread gaps of identical size and no noise the FFWVA functions with low errors comparable to the LWM.

5.2. Conclusion

The general conclusion of this thesis is that the proposed FFWVA can determine the horizontal wind parameters wind direction and wind speed correctly. The initial research statement stated that "An on a discrete Fourier transform based VAD approach can be used to perform wind field measurements and retrieve the horizontal wind speed and direction from an azimuthal Doppler radar scan". At this point the statement is only partly true: The FFWVA determines both the wind speed and wind direction but with an error that isn't correctable in all simulated cases. Under specific conditions, when an equal spread of gaps in the data is available and/or exactly 50% of the data is used as input, the determination of horizontal wind parameters is possible with a lower error.

A single gap causes a jump in the velocity round scan data from a value to zero and back to a correct value. These jumps are discontinuities in the signal and DFT input. The DFT and thus FFWVA

has difficulties with these inconsistent discontinuities caused by the single gap. The azimuthal starting position of the gap has an influence on the size of the errors of both the wind direction and the wind speed. The main cause of the errors in the FFWVA horizontal wind determination is due to spectral leakage to other frequency bins in the processed DFT. Minimizing spectral leakage was not in the scope of this research.

The low error when using exactly 50% of the data instead of the full 100% is an interesting case. The low error seems to achieved by a balanced spectrum where the DFT frequency bins are aligned to the DFT window. Unfortunately the exact reason for this optimum and the minimization of spectral leakage have not been investigated properly during this research.

If enough velocity data is available the FFWVA is able to retrieve the horizontal wind parameters correctly. When this data is available the FFWVA is able to retrieve the wind profile of a multi-layered wind fields successfully. Considering the computational power first tests indicate that the Matlab implementation of the fft function is less heavy or better optimized compared to Matlab's Isqlin function.

5.3. Recommendations

As the results shows that the FFWVA works with low error under specific circumstances new questions regarding the FFWVA capabilities arise. The expectation is that the FFWVA wind speed and direction determination errors can be kept low by selectively ignoring data, but additional work is needed to test this. Ideally that work should be combined with additional research on optimization of the DFT bin size or DFT window.

Another part that has not been researched yet is the investigation of the remaining DFT frequency bins (Fourier coefficients). Other than the first frequency bin used by the FFWVA the higher frequency bins could contain information on wind anomalies non-centered around radar. For example a wind vortex in a certain quadrant of the radar PPI.

Appendices



Criteria for KNMI weather warning codes

Drempelwaarden	voor de k	leurcodes
----------------	-----------	-----------

	Code geel	Code oranje
Regen :	Verkeershinder door aquaplaning, of >50 mm in 24 uur	>75 mm in 24 uur
Gladheid & sneeuw	Minimaal 1 van de volgende criteria: * lokale gladheid door op-, aan- of bevriezing van natte weggedeelten, hagel, sneeuwresten of lokale ijzel * tot 5 cm sneeuw in 6 uur * tot 3 cm sneeuw in 1 uur	Minimaal 1 van de volgende criteria: * op uitgebreide schaal gladheid door ijzel of bevriezing * >5 cm sneeuw in 6 uur * >3 cm sneeuw in 1 uur * sneeuwval en/of driftsneeuw (>40 km per uur), leidend tot sneeuwduinen
Onweersbuien 🔾	Lokale onweersbuien met lokaal één of meer van de volgende verschijnselen: * windstoten (>60 km per uur) * of lokaal veel neerslag (>30 mm in 1 uur) * of hagel (tot 2 cm)	Georganiseerde onweersbuien met lokaal één of meer van de volgende verschijnselen: * zware windstoten (>75 km/uur) * of lokaal veel neerslag (>50 mm in 1 uur) * of grote hagel (>2 cm)
Windstoten fa	>75 km per uur Kust, winter: 90 km per uur	>100 km per uur Kust, winter: 120 km per uur
Temperatuur (hitte/koude)	nittepian (4 dagen naximum temperatuur	Minimaal 1 van de volgende criteria: * drie aaneengesloten etmalen maximum temperatuur >30 °C, waarbij minimum temperatuur >18 °C * windchill < -20 °C
Zicht 😤	< 200 m	<10 m
Hozen 🥰	Bij waarneming (geen standaard tijdsduur)	

Verwachtingstermijn, kans en gebiedsgrootte

		Code rood (weeralarm) Uitgifte o.b.v. impactanalyse
	Code oranje Kans > 60%, gebied > 50 x Uitgifte o.b.v. overschrijden oranje na consultatie meteo	meteorologische criteria voor
Code geel Kans ≥ 60%, onafhankelijk van gebiedsgrootte Uitgifte o.b.v. overschrijden meteorologische criteria voor	geel	
48	24	12
→ Verwachtingstermijn (uren	tot aan optreden van het fenomeer)

Figure A.1: Criteria table of the KNMI for their weather warning system. The first part, above, shows different weather hazards as the different rows and their specific criteria for warning codes in the columns. The second part, below, is independent of the various hazards specifying the area and chance [26].

Bibliography

- [1] E. D. Craft, "An economic history of weather forecasting," Website, 2015. [Online]. Available: http://eh.net/encyclopedia/an-economic-history-of-weather-forecasting/
- [2] L. Alter, "Meteorology," Website, 2015. [Online]. Available: http://www.yale.edu/ynhti/curriculum/ units/1994/5/94.05.01.x.html
- [3] Infoplease.com, "Meteorology," Website, 2016. [Online]. Available: http://www.infoplease.com/ cig/weather/forecasting-from-beginning.html
- [4] R. Doviak and D. Zrnic, Doppler Radar and Weather Observations: Second Edition. 1250 Sixth Avenue, San Diego, California 92101-4311: Academic Press, INC., 1993.
- [5] V. (wiki), "Nexrad," Website, 2016. [Online]. Available: https://en.wikipedia.org/wiki/NEXRAD
- [6] —, "Microscale and macroscale models," Website, 2016. [Online]. Available: https://en.wikipedia.org/wiki/Microscale_and_macroscale_models
- [7] I. Orlanski, "A rational subdivision of scales for atmospheric processes," Bulletin of the American Meteorological Society, vol. Volume 56, no. Number 5, pp. 527–530, May 1975.
- [8] V. (wiki), "Microburst," Website, 2016. [Online]. Available: https://en.wikipedia.org/wiki/ Microburst
- [9] —, "Terminal doppler weather radar," Website, 2016. [Online]. Available: https://en.wikipedia. org/wiki/Terminal_Doppler_Weather_Radar
- [10] "Terminal doppler weather radar information," Website, 2016. [Online]. Available: http: //www.weather.gov/gsp/tdwr_specs
- [11] C. Collier, Applications of Weather Radar Systems. Market Cross House, Cooperstreet, Chichester, West Sussex, England: Ellis Horwood Limited, 1989.
- [12] K. Browning and R. Wexler, "The determination of kinematic properties of a wind field using doppler radar," *Journal of Applied Meteorology*, vol. 7, no. 1, pp. 105–113, February 1968.
- [13] R. A. Brown and V. T. Wood, "A guide for interpreting doppler velocity patterns: Northern hemisphere edition," NOAA / National Severe Storms Laboratory, Tech. Rep., 2007.
- [14] S. Kingsley and S. Quegan, Understanding Radar Systems. 89 Dean Road, Mendham, NJ 07945: SciTech Publishing, Inc., 1999.
- [15] A. C. P. Oude Nijhuis, C. M. H. Unal, O. A. Krasnov, H. W. J. Russchenberg, and A. Yarovoy, "Outlook for a new wind field retrieval technique: The 4d-var wind retrieval." Delft University of Technology, Tech. Rep., 2014. [Online]. Available: http://doi.org/10.1109/RADAR.2014.7060421
- [16] S. V. Vaseghi, *Advanced Digital Signal Processing and Noise Reduction*, 2nd ed. Baffins Lane, Chichester, West Sussex, PO19 1UD, England: John Wiley & Sons, Ltd, 2000.
- [17] A. Oude-Nijhuis, "Zephyros github source code," Website, 2016. [Online]. Available: https://github.com/albertoudenijhuis/zephyros0.4
- [18] A. B. Carlson, Communication Systems, 4th ed. 1221 Avenue of the Americas, New York, NY 10020: McGraw-Hill, 2002.
- [19] J. R. Taylor, An Introduction to Error Analysis: The Study of Uncertainties in Physical Measurements. 55D Gate Five Road, Sausalito, CA 94965: University Science Books, 1997.

- [20] Various, "Frequency domain," Website, 2016. [Online]. Available: https://en.wikipedia.org/wiki/ Frequency domain
- [21] T. H. Park, *Introduction to digital signal processing: computer musically speaking*. 5 Toh Tuck Link, Singapore 596224: World Scientific, 2009.
- [22] J. W. Cooley and J. W. Tukey, "An algorithm for the machine calculation of complex fourier series," *Mathematics of computation*, vol. 19, no. 90, pp. 297–301, 1965.
- [23] J. O. Smith, Mathematics of the Discrete Fourier Transform (DFT), 2nd ed. Music Department, Stanford University, Stanford, California 94305: W3K Publishing (self-published), 2007. [Online]. Available: https://ccrma.stanford.edu/~jos/mdft/
- [24] Various, "Fourier transform," Website, 2016. [Online]. Available: https://en.wikipedia.org/wiki/ Fourier_transform
- [25] M. Frigo and S. G. Johnson, "The design and implementation of FFTW3," *Proceedings of the IEEE*, vol. 93, no. 2, pp. 216–231, 2005, special issue on "Program Generation, Optimization, and Platform Adaptation".
- [26] "Weeralarm," Website, 2016. [Online]. Available: http://www.knmi.nl